

Human Endothelial Actin-binding Protein (ABP-280, Nonmuscle Filamin): A Molecular Leaf Spring

Jed B. Gorlin,*§ Rina Yamin,* Sheila Egan,* Murray Stewart,|| Thomas P. Stossel,* David J. Kwiatkowski,* and John H. Hartwig*‡

*Hematology Unit, Department of Medicine, and the ‡Department of Anatomy and Cellular Biology, Massachusetts General Hospital and **Harvard Medical School, Charlestown, Massachusetts 02129; §Hematology Division, Children's Hospital and Pediatric Oncology Division, Dana-Farber Cancer Institute, Boston, Massachusetts 02115; and ||Medical Research Council Laboratory of Molecular Biology, Cambridge CB2 2QH, England

Abstract. Actin-binding protein (ABP-280, nonmuscle filamin) is a ubiquitous dimeric actin cross-linking phosphoprotein of peripheral cytoplasm, where it promotes orthogonal branching of actin filaments and links actin filaments to membrane glycoproteins. The complete nucleotide sequence of human endothelial cell ABP cDNA predicts a polypeptide subunit chain of 2,647 amino acids, corresponding to 280 kD, also the mass derived from physical measurements of the native protein. The actin-binding domain is near the amino-terminus of the subunit where the amino acid sequence is similar to other actin filament binding proteins, including α -actinin, β -spectrin, dystrophin, and *Dictyostelium* abp-120. The remaining 90% of the sequence comprises 24 repeats, each \sim 96 residues long, predicted to have stretches of β -sheet secondary structure interspersed with turns. The first 15 repeats may have substantial intrachain hydrophobic interactions and overlap in a staggered fashion to yield a backbone with mechanical resilience. Sequence insertions immediately before repeats 16 and 24 predict two

hinges in the molecule near points where rotary-shadowed molecules appear to swivel in electron micrographs. Both putative hinge regions are susceptible to cleavage by proteases and the second also contains the site that binds the platelet glycoprotein Ib/IX complex. Phosphorylation consensus sequences are also located in the hinges or near them. Degeneracy within every even-numbered repeat between 16 and 24 and the insertion before repeat 24 may convert interactions within chains to interactions between chains to account for dimer formation within a domain of 7 kD at the carboxy-terminus. The structure of ABP dimers resembles a leaf spring. Interchain interactions hold the leaves firmly together at one end, whereas intrachain hydrophobic bonds reinforce the arms of the spring where the leaves diverge, making it sufficiently stiff to promote high-angle branching of actin filaments. The large size of the leaves, their interruption by two hinges and flexible actin-binding site, facilitate cross-linking of widely dispersed actin filaments.

NONMUSCLE cells achieve a wide variety of shapes by arranging peripheral linear actin filaments in different ways. Actin-modulating proteins are responsible for this versatility by adjusting actin filament length and by defining the organization of actin filaments and their binding to other cellular components (54, 56). Actin-binding protein (ABP, also called nonmuscle filamin)¹ was among the first such proteins discovered (25, 55, 62) and has a broad phylogenetic distribution (3, 4, 34, 47, 49, 51, 59, 60, 63). ABP from most cell types examined promotes high-angle

branching of actin filaments (24, 27, 40), an attribute initially inferred from its potency in initiating the gelation of actin filament solutions (6, 26). Smooth muscle ABP (filamin) from chicken gizzard, on the other hand, causes bundling of actin filaments despite extensive immunologic and hydrodynamic similarity with ABP from other cells (6, 14, 45).

Since rodlike linear polymers tend to align in parallel when the local concentration is high, it is not surprising that most actin-cross-linking proteins stabilize actin filament bundles. However, ABP is remarkable in generating near perpendicular branching of long helical actin filaments. Previous analysis of ABP's structure gave some insights into how this is done. Hydrodynamic and electron microscopic analyses have showed ABP to be a homodimer (26), with subunit size 270 kD and dimensions of 3–5 nm width and

Address correspondence to Jed B. Gorlin, Hematology Research Unit 8W, Massachusetts General Hospital, Building 149, 13th Street, Charlestown, MA 02129.

1. *Abbreviations used in this paper:* ABP, actin-binding protein; DMA, dimethyl adipimate; HUVEC, human umbilical vein endothelial cells.

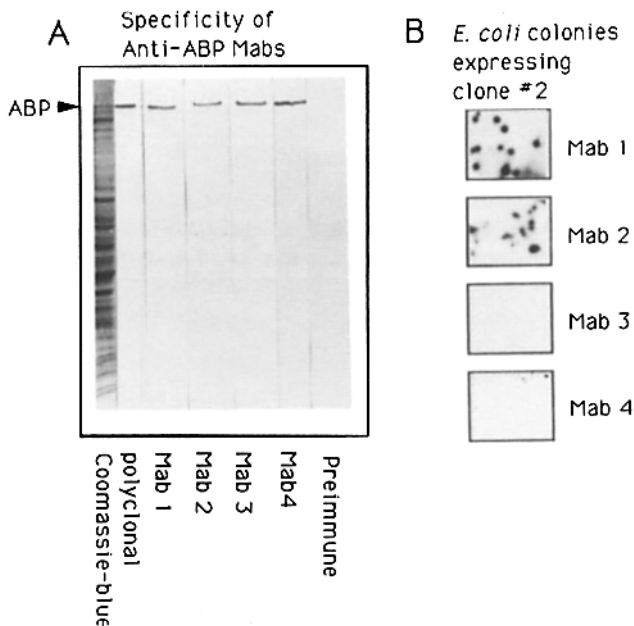


Figure 1. (A) Specificity of mouse monoclonal IgGs 1-4 for ABP and (B) demonstration that mAbs 1 and 2, but not 3 and 4, bind to the fusion protein encoded by λ gt11 clone 2. (A) Rabbit lung macrophages were dissolved with 1% SDS and polypeptides displayed by SDS-PAGE, electrophoretically transferred to nitrocellulose paper, and immunoblotted against each mAb followed by peroxidase-conjugated secondary IgG. Only the high molecular weight subunit of ABP is recognized by each of the mAb (B) Autoradiograph showing that only mAbs 1 and 2 recognize the λ gt11 clone 2 fusion protein. Colonies were blotted on nitrocellulose paper, incubated with each monoclonal IgG followed by 125 I-anti-mouse IgG.

160 nm length (26, 58). Because subunits contain both self-association and actin-binding sites, the intact molecule can crosslink two actin filaments. Electron micrographs suggested that subunit self-association involved an end-to-end attachment of the filamentous strands and actin binding occurred at the distal portion of each free end of the ABP molecule, which seemed to attach to the groove between the long-pitch strands of the actin helix. It was proposed that the large size of ABP and separation of its actin-binding sites were prerequisites for the orthogonal cross-linking of actin filaments. Recent rheologic studies of ABP/actin gels confirm that they resemble covalently crosslinked networks and display considerable elastic properties in contrast to gels made from actin alone (30).

ABP also mediates the association of cytoskeletal actin with the plasma membrane protein GPIb/IX complex of human blood platelets (20, 43) and with a glycoprotein in other cell-types. Therefore ABP molecules have a binding site for integral membrane glycoproteins, as well as self-association and actin filament binding domains. In addition, ABP is a phosphoprotein, whose extent of phosphorylation changes in response to cell activation (8, 9, 59).

This paper reports the complete primary sequence of ABP inferred from cDNA clones and the identification of its functional domains by mapping of proteolytic fragments with mAbs and by functional analysis of genetically engineered fragments secreted by Cos cells. The observations suggest how ABP can cause high-angle branching of actin filaments.

Materials and Methods

Mouse IgG mAbs against ABP

Mouse mAb to rabbit macrophage, and human platelet and uterus ABP were produced. Balb/C mice were immunized every 3 wk with a total of four injections of 50 μ g of ABP, the first in CFA, the latter three in incomplete Freund's adjuvant (1 vol ABP in PBS/1 vol adjuvant). A final boost of 20 μ g of ABP in PBS was injected into the tail vein 3 d before splenectomy. Homogenized spleen cells were fused with P3-NS1-Ag4-1 myeloma cells with 30% polyethylene glycol (M_r 1,000). Hybridomas secreting antibodies specific for ABP were identified by ELISA assay of ABP coated wells. 96-well microtiter plates were coated with 50 μ l of 5 μ g/ml of actin-binding protein in 10 mM sodium bicarbonate buffer, pH 9.6 for 2 h. 50 μ l of culture medium was added to each well and incubated at room temperature for 2 h. The test solutions were removed and wells washed with PBS containing 0.2% Tween. Bound IgG was identified with peroxidase-labeled goat anti-mouse IgG. Secreting hybridoma cells were subcloned twice by limiting dilution, and injected peritoneally into pristane-primed mice. Antibodies were purified from ascites fluid, obtained 7-10 d after injecting hybridoma cells, by precipitation with 45% ammonium sulfate and ion exchange chromatography on DEAE-Sepharose.

Four IgG mAbs specific for rabbit macrophage, human uterine, and platelet ABP were prepared and designated mAbs 1-4. Fig. 1 shows an immunoblot illustrating the specificity of each antibody for rabbit macrophage ABP. Total macrophage proteins were solubilized in SDS, polypeptides separated by electrophoresis through 5-15% polyacrylamide slab gels, transferred to nitrocellulose membrane and incubated with each mAb (57). In all cases, IgGs bound only the high molecular weight subunit of ABP. Identical results were obtained using extracts of human uterus (data not shown). The binding location of each mAb was mapped on the ABP subunit in proteolytic studies (Fig. 4 c).

Protein Purification, Proteolysis of ABP, and Amino-Terminal Peptide Sequencing of Proteolytic and Chemical Fragments

ABP was purified from human uterus as previously described (26). Purified ABP was proteolysed with calpain and trypsin. Calpains I and II were generous gifts from Dr. Dorothy Croall (Department of Physiology, University of Texas Health Science Center) and Dr. Darell Goll (University of Arizona, Muscle Biology Group), respectively.

Digestion with Calpain. Purified human uterus ABP in 0.1 M KCl, 0.5 mM DTT, and 10 mM imidazole-HCl, pH 7.5 was incubated with calpain at a weight ratio of 100 ABP:1 calpain for 0-60 min at room temperature. Proteolysis was initiated by the addition of calcium to a final concentration of 2 mM and quenched with EGTA at a final concentration of 5 mM. The enzymatic digest was subjected to 5-15% SDS-PAGE and transferred to Immobilon-P.

Digestion with Trypsin. Human ABP in 0.1 M KCl, 10 mM imidazole-HCl, 0.1 mM EGTA, 1 mM DTT pH 7.5, was digested with TPCK-trypsin (Sigma Chemical Co., St. Louis, MO) using a final molar ratio of 25 mol of ABP:1 mol trypsin for 0-60 min at room temperature. The digestion was stopped at times of 0, 5, 15, 40, and 60 min by adding soybean trypsin inhibitor (Sigma Chemical Co.) at equal weight to trypsin. The enzymatic digest was subjected to 5-15% SDS-PAGE and transferred to Immobilon-P (Millipore Corp., Bedford, MA) by Western blot.

Protein Sequencing. Western blots from both tryptic and calpain digests and cyanogen bromide-cleaved ABP were stained with Coomassie brilliant blue and the 100-kD band from the Calpain digest and selected bands from the tryptic digest and chemical cleavage were excised and sequenced (38).

Binding of ABP and its Proteolytic Subfragments to Actin

An F-actin cosedimentation assay was used to determine which tryptic or calpain fragments bound actin filaments. Increasing concentrations of intact human uterine ABP (control) or ABP digests were mixed and incubated with 100 μ l of 3 μ M F-actin in 0.1 M KCl, 2 mM MgCl₂, 0.1 mM EGTA, 0.5 mM β -mercaptoethanol, 10 mM imidazole-HCl, pH 7.5 for 30 min at room temperature. Samples were centrifuged at 200,000 g for 15 min (model TL-100 centrifuge; Beckman Instruments, Fullerton, CA) at 4°C, separated into supernatants and pellets, solubilized in gel sample buffer, and electrophoresed on 5-15% polyacrylamide slab gels in the presence of 0.1% SDS. ABP in each sample was quantitated by densitometric scanning after

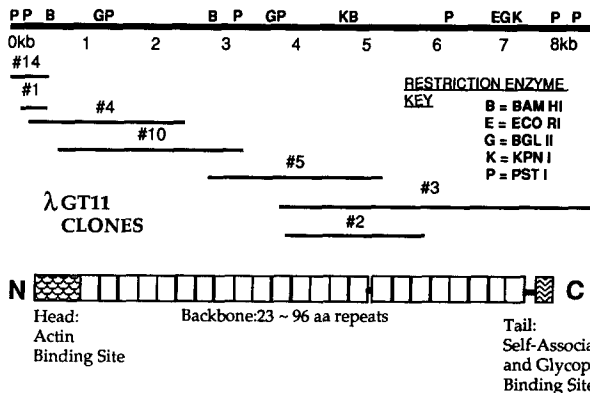


Figure 2. Sequencing strategy of human ABP and alignment of overlapping cDNA clones. All clones were isolated from human endothelial cell λ gt11 libraries. The original isolate was clone 2. The location of important restriction enzyme sites is indicated. The diagram aligns the ABP cDNA with important functional domains of the ABP subunit.

Coomassie brilliant blue staining. Subfragments of ABP retaining F-actin binding activity (sedimented with F-actin) were aligned relative to the intact subunit by immunoblotting with the panel of anti-ABP mAbs.

EM of Human Uterus ABP

ABP at a concentration of 50 μ g/ml in 50% glycerol containing 0.1 M KCl, 0.1 mM EGTA, 0.1 mM DTT, and 10 mM imidazole-HCl, pH 7.5 was sprayed onto freshly cleaved mica (58), vacuum dried, and rotary coated with tantalum-tungsten at 5° and carbon at 90° in a freeze-fracture machine (model CFE-50; Cressington, Watford, England). Replicas were floated from the mica in 50% hydrofluoric acid, washed in water, and picked up on copper grids.

cDNA Cloning

Escherichia coli expressing β -galactosidase-ABP fusion proteins directed by infection with human umbilical vein endothelial cell (HUVEC) cDNA libraries in λ gt11 (both oligo dT and randomly primed cDNA libraries were generously provided by Dr. Stuart Orkin) (22) were initially identified using a mixture of anti-ABP mAbs 1 and 2 and 125 I-labeled secondary rabbit anti-mouse IgGs. Clone 2, the original isolate, was subsequently shown to be recognized by each of the individual mAbs 1 and 2 (Fig. 1). Its cDNA insert was isolated from the recombinant phage by standard methods (36), subcloned into M13 (39), and sequenced using the dideoxy method of Sanger (48). Where restriction sites were lacking, serial deletions were created in the cDNA subcloned into plasmid vectors pUC13 (Bethesda Research Laboratories, Gaithersburg, MD) and Bluescript SK+ (Stratagene Corp., La Jolla, CA) using the Exonuclease III method of Henikoff (28). The resultant deleted plasmids were sequenced after subcloning into M13, or directly sequenced using synthetic oligonucleotide primers derived from either vector or ABP sequence. The libraries were rescreened with probes from either end of clone 2. Through a series of rescreenings, seven overlapping clones spanning 8.4 kb were isolated and sequenced in both directions (Fig. 2). More than 300 bp of identical overlapping sequence in both directions was used to document that each new clone represented a contiguous cDNA sequence. Clone 1 in Fig. 2 was subcloned from λ gt11 using the polymerase chain reaction (PCR). A toothpick was applied to plaques, added to a standard PCR mix (16), and heated 5 min at 95°C to destroy DNases. 30 cycles of amplification were performed using an antisense oligonucleotide and a λ gt11 forward or reverse primer. To ensure sequence fidelity during amplification, four separate clones were sequenced.

Northern Analysis

Total cellular RNA derived from human white blood cells, uterus, a hepatoma (G2) cell line, and rabbit alveolar macrophages was prepared by the guanidium thiocyanate method (10). Fresh tissue was combined with 4 M guanidium thiocyanate, homogenized, and layered onto a 5.7 M CsCl cushion and centrifuged at 35,000 rpm (115,000 g) for 8 h. The pelleted RNA

was ethanol washed, resuspended, ethanol precipitated, and quantitated spectrophotometrically after resuspension in a Tris EDTA buffer. 10 μ g total cellular RNA (per lane) was electrophoresed through a denaturing 2.2 M formaldehyde, 1% agarose gel, and transferred via capillary blotting to a synthetic support (Genescreen; New England Nuclear, Boston, MA). The transferred RNA was analyzed by hybridization with probes prepared from the various ABP cDNA clones.

Cos Cell Expression of ABP Truncates

cDNA encoding regions within ABP's carboxyl- and amino-ends were subcloned into the CDM8 plasmid (50). This Cos cell expression vector yields high transient expression of transfected protein constructs. The self-association domain of ABP was mapped to the carboxy-terminal repeat by creating two hybrid constructs including repeat motifs 21–24 (henceforth named 21E–24H = residues 2,282–2,647) or repeat motifs 21–24 with the last 65 residues deleted (21E–24C = residues 2,282–2,582), subcloned into the CDM8-PLGE plasmid. The former construct included the native ABP stop codon whereas the latter construct was formed by ligating the Pst I site (base \sim 7,993) to the Pst I site in the CDM8 polylinker region that encodes a hexapeptide RSRPRL before an in-frame stop codon. Each transfected construct encoded a fusion protein incorporating the amino-terminal 40 amino acids of plasma gelsolin including its signal peptide (that is cleaved off during the secretion process) and 12 residues unique to its plasma extension (relative to cytoplasmic gelsolin). The proteins produced are both secreted into the media and identifiable using a rabbit antibody generated against a synthetic peptide composed of the first 15 residues of plasma gelsolin. A cDNA construct encoding ABP residues 183–689 was similarly fused to the plasma gelsolin cDNA (again encoding the amino-terminal 40 residues) after addition of synthetic oligonucleotide "three-frame stop codon" linkers to the 3' terminus of the partial ABP cDNA and subcloned into the CDM8 plasmid. Hybrid constructs were transfected into Cos cells using dextran followed by DMSO shock. The cells were allowed to grow for 16–24 h in 10% serum-containing media then washed in HBSS (Gibco Laboratories, Grand Island, NY) and grown for 48 h in serum-free media. The serum-free media was collected over a 48-h span, dialyzed in 1,000 volume of 10 mM Tris, pH 7.4, containing 1 mM DTT and 5 mM EGTA and freeze-dried.

Chemical Cross-linking of the Expressed ABP Truncates

The freeze-dried Cos cell media containing the expressed proteins were resuspended in 0.15 ml of 0.5 M KCl, 200 mM triethanolamine pH 8.5 and 1% β -mercaptoethanol, dialyzed against the same and clarified by centrifugation in an ultracentrifuge (TL-100; Beckman Instruments) at 106,000 g for 15 min at 4°C. Aliquots were removed for SDS-PAGE (uncross-linked control) and dimethyl adipimate (DMA) dissolved in the triethanolamine buffer was added at concentrations of 2.5 and 5 mg/ml. Samples were incubated with crosslinker for 2 h at 37°C. The reaction was stopped by boiling in SDS containing sample buffer and electrophoresed through 5–15% polyacrylamide slab gels in the presence of 0.1% SDS. Polypeptides were electrophoretically transferred to Immobilon-P, nonspecific protein binding sites blocked with 5% nonfat dry milk (Carnation, Los Angeles, CA) and ABP truncates identified using anti-amino-terminal plasma gelsolin IgG and anti-ABP mAb IgGs and peroxidase-labeled secondary antibodies.

Computer/Fourier Analysis of the Sequence

The nucleotide and protein sequence of ABP was analyzed using programs available to users of Bionet/Intelligenetics, the University of Wisconsin Genetic Computer Group (UWGCG) Programs and by Fourier analysis to detect regularly repeating motifs (53). Manipulations of the primary sequence were performed using SEQED and comparisons with COMPARE and DOTPLOT programs (UWGCG; [35]). Secondary structure predictions were analyzed according to the method of Chou-Fasman (12) and Robson and Suzuki (44); via the programs PEPTIDESTRUCTURE and PLOT-STRUCTURE (UWGCG). Database searches included those available via UWGCG. Comparison of the amino terminus of ABP with other actin-binding proteins and alignment of the 24 repeats used iterative applications of the GAP, LINEUP and PRETTY programs on UWGCG. Fourier transforms were calculated (41) scoring secondary structure according to Robson and Suzuki (44).

Table I. Predicted Amino Acid Composition of Human Endothelial Cell ABP Compared with Amino Acid Composition of Rabbit Macrophage ABP and Chicken Gizzard Filamin

| Amino acid | Human ABP | Rabbit ABP* | Chicken gizzard filamin‡ |
|------------|-----------|--------------|--------------------------|
| | | <i>mol %</i> | |
| ALA | 7.2 | 7.4 | 9.3 |
| CYS | 1.8 | 0.5 | 2.0 |
| ASP/ASN | 8.4 | 8.7 | 7.6 |
| GLU/GLN | 9.6 | 11.4 | 9.5 |
| PHE | 2.9 | 3.2 | 2.9 |
| GLY | 11.4 | 11.8 | 12.5 |
| HIS | 2.5 | 2.1 | 2.3 |
| ILE | 4.2 | 4.4 | 3.3 |
| LYS | 6.0 | 6.0 | 4.8 |
| LEU | 5.3 | 6.2 | 6.0 |
| MET | 1.1 | 1.3 | 0.8 |
| PRO | 7.9 | 7.1 | 8.0 |
| ARG | 3.5 | 4.1 | 5.5 |
| SER | 7.0 | 6.8 | 6.8 |
| THR | 6.6 | 6.2 | 5.3 |
| VAL | 10.5 | 8.5 | 10.0 |
| TRP | 0.6 | 1.1 | 1.0 |
| TYR | 3.2 | 3.1 | 2.6 |

* Stossel and Hartwig (1976); ‡ Wang (1977).

Because the ABP amino terminus is blocked, we could not use direct amino acid sequencing to confirm the location of the initiation methionine. However, two considerations indicate that the position chosen in Fig. 3 is correct. First, 60–70 bases upstream of the proposed initiation codon are stop codons in all three frames. The methionine at residue 28 is also a potential initiation site, although the presence of another in-frame ATG upstream from a documented initiation site, without interposing termination codons, is unusual. Second, the predicted amino acid sequence at the proposed amino-terminus of ABP is similar to that found at the amino-terminus of α -actinin (1, 66), a *Dictyostelium* actin cross-linking protein (41) designated abp-120 by Condeelis (13), dystrophin (23), and the β -chain of nonerythroid spectrin (7). Neither initiation sequence is flanked by the initiation consensus sequence (CCA/GCCAUGG) (32). Therefore, assignment of the true initiation codon between methionine 1 or 28 is tentative until more definitive evidence can be obtained.

Molecular Organization of ABP

High-resolution electron micrographs of ABP molecules (Fig. 4 b) show that they are constructed from two elongated chains that dimerize at one end, which we call the tail and which we now know corresponds to the carboxy-terminus of each chain. Accordingly, an ABP monomer can be divided into three principal domains: an actin-binding head, an elongated rod-like backbone, and a tail containing the dimerization site (Fig. 4 a). In the following sections, we will detail how many of these properties can be accounted for in terms of the primary structure of ABP. We show that the head has a primary structure related to the amino-terminal domains of several other actin-binding proteins, whereas the backbone or rod domain contains 24 tandem repeats, containing

on average 96 amino acids, which account for the extended molecular structure of ABP. Moreover, systematic variations in the internal structure of these 96-residue repeats suggest a mechanism for chain dimerization and also a model, based on a leaf spring, that accounts for several properties of ABP-actin networks.

Location of ABP Functional Domains

The location of the different functional domains of ABP in the amino acid sequence was defined by using anti-ABP mAbs to map a range of proteolytic fragments and portions of ABP expressed in Cos cells. Once these fragments had been mapped, specific functions, such as actin-binding and dimerization, could be assessed and so assigned to defined regions of the sequence. Fig. 4 c summarizes the mapping data for ABP.

As shown previously (18, 21, 64), proteolysis of ABP with calpain yielded fragments of 190, 100, and 90 kD (Fig. 5 a). Amino acid sequencing of the amino-terminal of the 100 kD fragment (TYA) located this calpain site between residues 1,761 and 1,762, therefore the 190 and 100 kD fragments derived from the amino- and carboxy-termini of the chain, respectively. mAbs 1 and 2 bound to both the 100- and 90-kD calpain fragments (showing that the 90-kD fragment derived from the 100-kD fragment), whereas mAbs 3 and 4 bound the 190-kD fragment (Fig. 5 b). Proteolysis of ABP with trypsin gave a more complex pattern of fragments, although two general patterns emerged. The initial cleavage resembled that with calpain and produced large (150–170 kD) and small (90–100 kD) fragments (Fig. 6 a). More extended proteolysis resulted in a series of polypeptides of sizes that were roughly multiples of 10 kD (Fig. 6 a), which indicated the presence of repeated cleavage sites spaced \sim 100 residues apart. As shown in Figs. 5 and 6, the 190-kD calpain fragment and the 170- and 90-kD tryptic fragments were all recognized by mAbs 3 and 4. The location of the mAb 4 epitope was defined more precisely by expressing cDNA corresponding to residues 183–689 of ABP as a hybrid protein in Cos cells. The expressed protein was recognized by mAb 4, but not mAb 3, and did not cosediment with F-actin (data not shown). Therefore, the epitope for mAb 4 was located between 20 and 75 kD from the ABP amino terminus. mAb 3 recognized 90- and 70-kD tryptic fragments, of which only the first bound actin. These data indicated that the epitope for mAb 3 was probably located towards the carboxy-terminus of the 90-kD calpain and tryptic fragments.

The Head Domain Binds F-Actin and Shares Homology with the Amino-Terminal Domains of Several Other Actin-binding Proteins

The actin-binding properties of fragments of ABP localized the actin-binding site to near the amino terminus of the sequence. Fig. 7 compares the F-actin binding affinity and stoichiometry of intact ABP with calpain fragments using an actin cosedimentation assay. Both intact ABP and the 190-kD fragment pelleted with F-actin, whereas the 100- and 90-kD fragments remained soluble. ABP bound to F-actin with a K_{app} of 1 μ M and capacity of 1 per 13.5 actin monomer subunits, consistent with previously published binding data (26). The affinity of the 190-kD fragment was diminished about threefold (calculated as a dimer for direct comparison

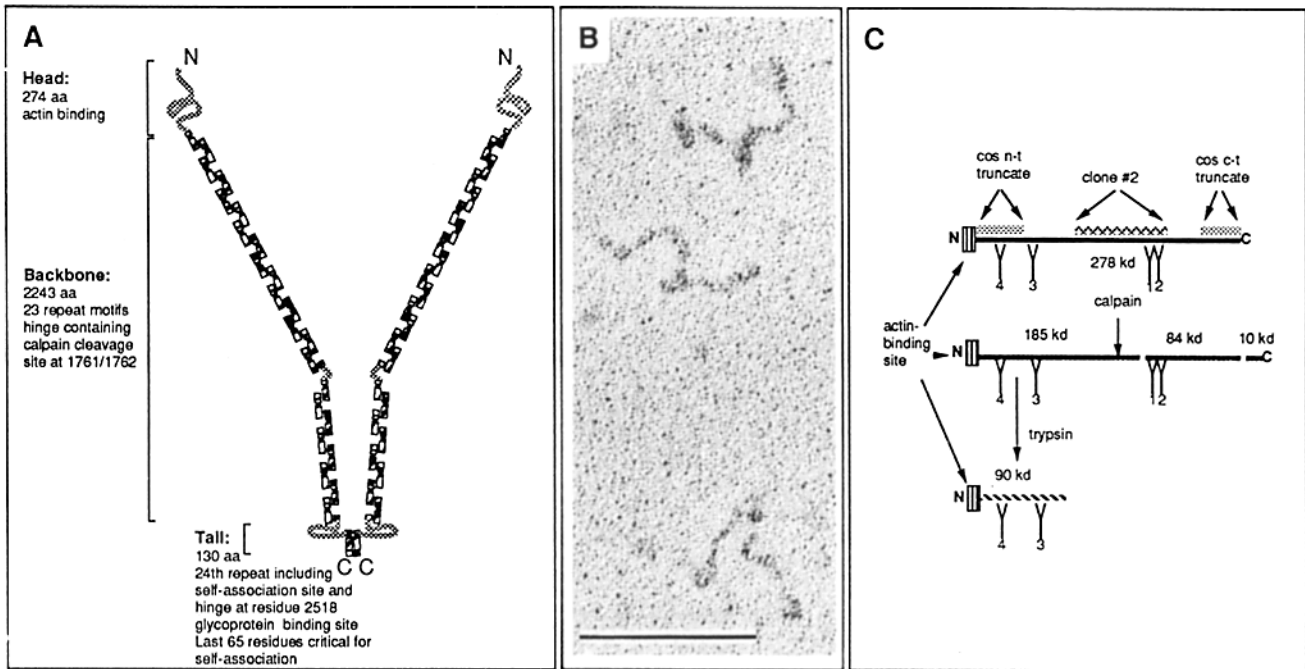


Figure 4. (A) Schematic model of the predicted dimeric structure of the ABP molecule. Each monomer chain contains three domains: head, backbone, and tail. Each head contains an actin filament binding site within 274 residues of the amino-terminus. The backbone contains repeat blocks of 96 amino acids composed of the last half of each sequence repeat and the beginning of the following sequence repeat (see Discussion and Figs. 9 and 10 for derivation of this functional repeat). Repeats associate through hydrophobic intrachain bonding until repeat 16 which is preceded by a 25-residue insertion that contains a calpain cleavage site. This region may act as a flexible hinge allowing movement of ABP's heads to accommodate actin-binding. Intra-repeat bonding continues in motifs 16–23 and completes the backbone of the subunit. The tail region (motif 24) is offset by a large ~ 35 amino acid insertion and the repeat abruptly terminates before the end of a functional repeat, thereby disrupting further intrachain bonding. The unpaired hydrophobic surfaces of motif 24 from two ABP subunits therefore are free to self-associate. Alternative models for ABP's structural repeat are described in the text. (B) Human uterus ABP molecules after glycerol spraying, vacuum drying, and metal coating with tantalum-tungsten at 5°. Note the minimal region of monomer overlap. Bar, 0.1 μm . (C) Summary of studies aligning ABP's functional domains within its primary sequence. The approximate binding location of mAbs 1–4 (schematically drawn as Ys with numbers), important proteolytic fragments, and regions that have been expressed in bacteria and Cos cells are shown. These data are presented in detail in Figs. 5–7. Calpain cleaves ABP into three pieces. The 187-kD fragment (190 kD by SDS-PAGE) contains the actin-binding site and ABP's amino terminus. A smaller 90-kD fragment can be made with trypsin that also contains ABP's amino terminus and binds actin. Smaller fragments of ABP with actin-binding activity have not been identified.

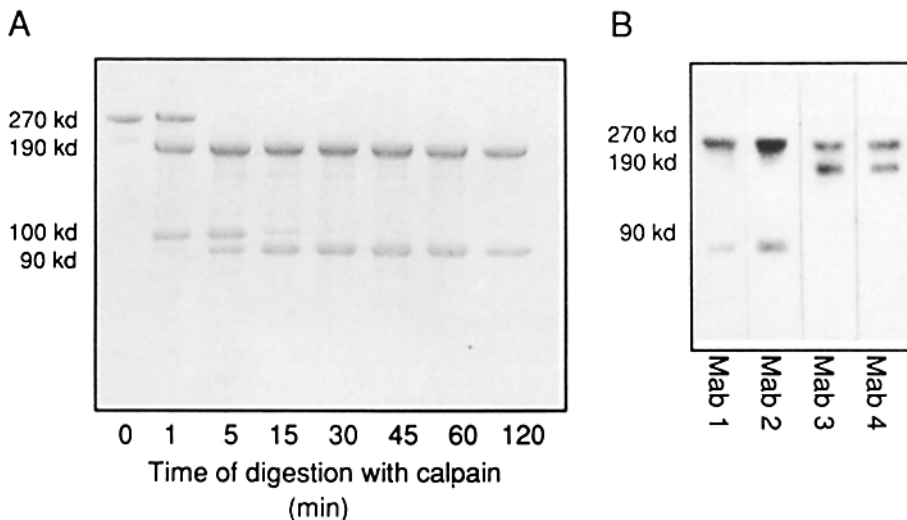


Figure 5. Evidence that ABP's amino terminus corresponds to its free molecular ends and contains the actin-binding site. Human uterus ABP, in 0.1 M KCl, 0.5 mM DTT, 1 mM CaCl_2 , and 10 mM imidazole-HCl, pH 7.5, was digested with calpain at a molar ratio of 1 calpain:25 ABP molecules. Cleavage was terminated by the addition of EGTA to a final concentration of 2 mM at the indicated times. The 270-kD ABP polypeptide is rapidly cleaved by smooth muscle calpain into 190- and 100-kD subfragments. With longer digestion, a 10-kD piece is subsequently cleaved from the end of the 100 kD subfragment. The 90-kD subfragment formed by this second cleavage, as well as the 190-kD piece, are resistant to further calpain cleavage. The sequence at the

190/100-kD junction (TYA) determined by direct protein sequencing is located at residues 1,762–1,764 in the translated ABP sequence. The 100-kD fragment, therefore, includes ABP's carboxy terminus, and the 190-kD fragment, its amino terminus. (B) Autoradiographs demonstrating that mAbs 1 and 2 and 3 and 4 recognize different ends of the ABP subunit. Fragments from a 30-min calpain digestion were transferred to Immobilon paper and blotted against each anti-ABP mAb 1–4 followed by ^{125}I -anti-mouse IgG. mAbs 1 and 2 recognize the carboxy-terminal 90-kD subfragment and mAbs 3 and 4 bind to the 190-kD amino-terminal subfragment.

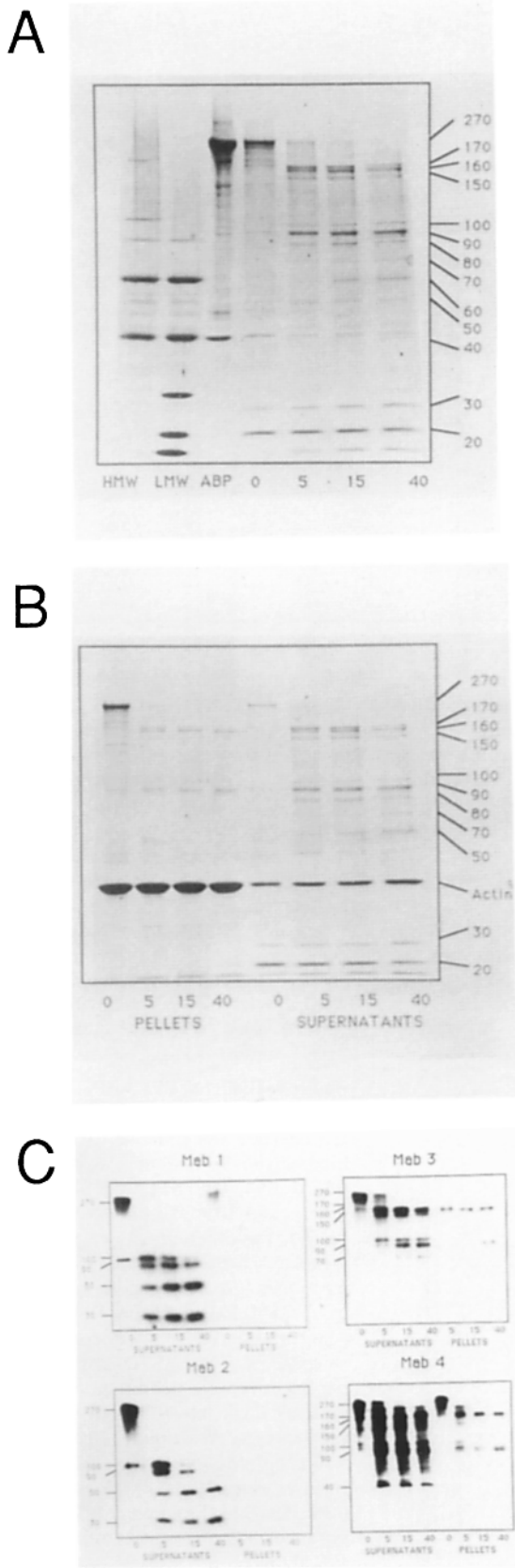


Figure 6. Fragmentation of human ABP with trypsin and identification of fragments that bind F-actin. (A) Time course for the cleavage of ABP by trypsin. ABP was digested with trypsin at a molar ratio of 25 ABP:1 trypsin at 4°C. Cleavage was stopped by addition of soybean trypsin inhibitor at the times indicated and the resulting

with ABP), but its capacity changed slightly from 13.5–16 actin monomers (also on a dimer basis, which would correspond to 8 actin monomers per fragment). The 90-kD tryptic fragment, which bound mAb 4, also sedimented with F-actin (Fig. 6 c). Combining the actin-binding activity of the proteolytic fragments with their mapping by monoclonal antibodies, the actin-binding site was localized to the amino-terminal third of each ABP monomer (Fig. 4 c).

As illustrated in Fig. 8, there was substantial similarity between the amino-terminal 275 residues of ABP and corresponding residues in several other actin-binding proteins such as α -actinin (1, 66), the β -chain of nonerythroid spectrin (7), and *Dictyostelium* abp-120 protein (41). It is likely, therefore, that a similar function is located at ABP's amino terminus. The greatest degree of homology between the sequences was found at positions 44–54, 67–74, 99–150, and 235–265 in the ABP sequence.

The Rod-like Backbone of ABP Contains Multiple Tandem Repeats

Dot matrix analysis of the ABP amino acid sequence (Fig. 9 a) indicated that there were 24 tandem repeats of a motif with an average length of ~ 96 residues. This repeating pattern began at residue 276 and continued to the carboxy terminus. Fig. 9 b shows an optimized alignment of these repeating motifs.

Interruptions in the Pattern of Tandem Repeats Indicate Flexible "Hinge" Regions in the ABP Rod Domain

The regular pattern of tandem repeats in the rod domain was interrupted in five places. These interruptions produced characteristic horizontal and vertical gaps in the dot-matrix plot (Fig. 9 a) and were apparent when the repeating motifs were aligned (Fig. 9 b). Insertions of 20–40 residues immediately before repeat motifs 16 and 24, and a 9-residue deletion at the amino terminus of repeat 18 account for three of the gaps. The insertion before repeat 16 contains the site of initial calpain proteolysis (see Figs. 3 and 5). The amino acid sequence of the initial portions of repeats 20 and 22 also show deviation from the consensus repeat, contributing to the apparent gaps on the dot-matrix analysis.

polypeptides displayed by SDS-PAGE and stained with Coomassie brilliant blue. The ABP subunit is attacked by trypsin in a stepwise fashion, i.e., polypeptides decrease by 10-kD steps consistent with the length of the ABP repeat motif. Molecular weight standards (Biorad Laboratories, Richmond, CA) from top to bottom are: *HMW* = 200, 116, 97, 66, and 42 kD; *LMW*: 97, 66, 42, 31, 21, and 14 kD. (B) Binding of trypsin cleavage fragments to F-actin demonstrating that fragments with sizes ~ 170 and 90 kD, that derive from the amino terminus, bind actin. Digests prepared as in A were mixed with F-actin, and F-actin was collected by pelleting at 200,000 g for 15 min in a centrifuge (TL-100). Soluble and pelleted material were subjected to SDS-PAGE followed by Coomassie brilliant blue staining or (C) electrophoretically transferred to Immobilon paper and immunoblotted against mAbs 1–4 followed by ^{125}I -anti-mouse IgG. The immunoblots (autoradiographs) demonstrate that only mAbs 3 and 4 recognize 170- and 90-kD fragments from ABP's amino terminus that bind F-actin. The 90 kD fragment derives, therefore, from fragmentation of the larger 170-kD fragment and an actin binding site must be within ≤ 90 kD of ABP's amino terminus.

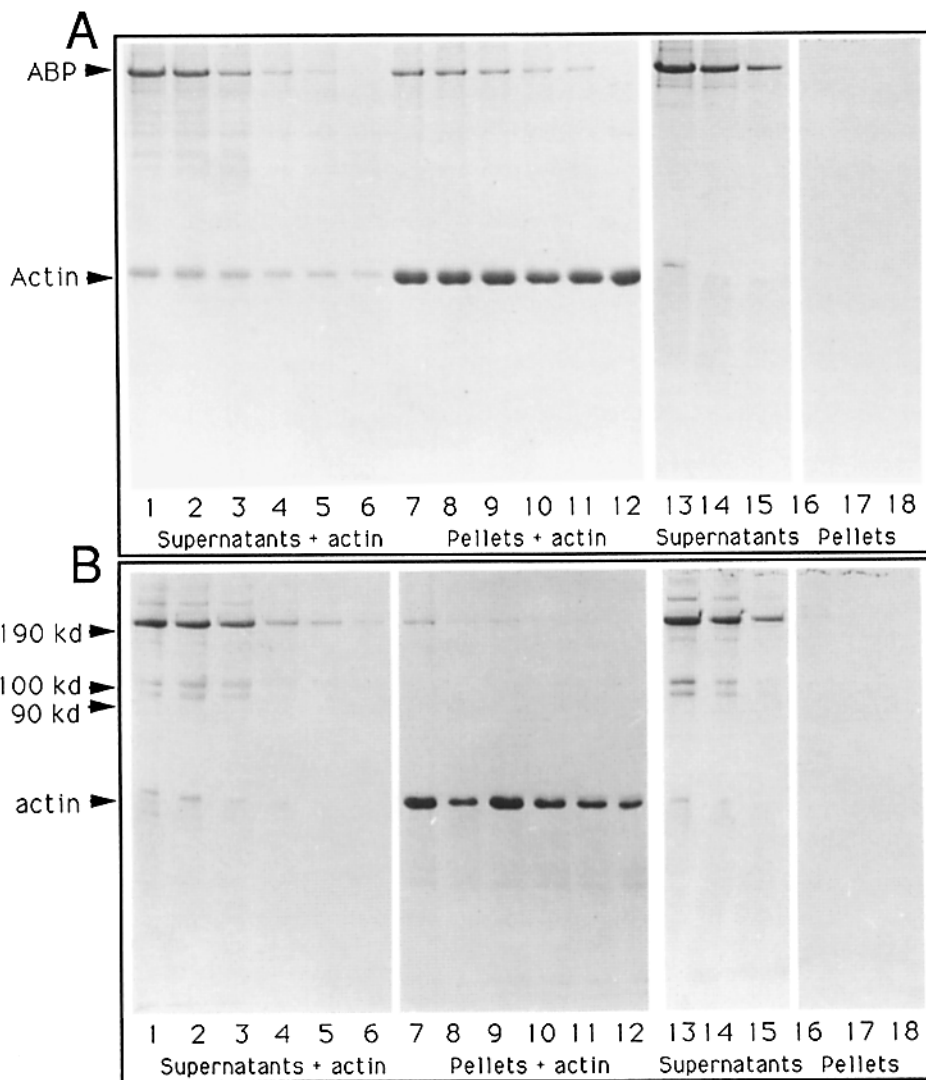


Figure 7. Binding of calpain-cleavage fragments of ABP to F-actin. As shown in Fig. 5, calpain cleaves ABP into fragments of 190 and 100/90 kD. We determined which cleavage fragment binds actin and compared its binding activity to native protein. Human uterine ABP in 0.1 M KCl solution of Fig. 5 was cleaved with calpain and actin co-sedimentation assays were performed as described in Materials and Methods. (A) Binding of ABP mixed with calpain in the presence of 1 mM EGTA. The SDS-PAGE shows supernatants (1–6) and pellets (7–12) of increasing concentrations of ABP incubated and cosedimented with 1 μ M rabbit skeletal muscle F-actin. The concentrations of ABP incubated with actin were 180 (lanes 1 and 7), 120 (lanes 2 and 8), 60 (lanes 3 and 9), 30 (lanes 4 and 10), and 15 (lanes 5 and 11) nM. Lanes 6 and 12 show actin without added ABP. ABP in the absence of actin (lanes 13–18) did not sediment. Concentrations of ABP in control lanes are 180 (lanes 13 and 16), 120 (lanes 14 and 17), and 60 nM (lanes 15 and 18). (B) SDS-PAGE showing that only the 190-kD subfragment binds F-actin. The supernatants (1–6) and pellets (7–12) after a calpain digestion and actin cosedimentation are shown. The concentrations of ABP digested and mixed with actin were 180 (lanes 1 and 7), 120 (lanes 2 and 8), 60 (lanes 3 and 9), 30 (lanes 4 and 10), 15 (lanes 5 and 11), and 7.5 nM (lanes 6 and 12). Calpain cleavage fragments do not sediment in the absence of added actin (control lanes 13–18). Concentrations of ABP are identical to corresponding lanes in A. (C) Scatchard plot comparing the binding affinities and capacities of the 190-kD polypeptide and native ABP to F-actin. The content of 190-kD in the supernatant and actin pellet were determined by densitometric scanning of Coomassie brilliant blue-stained SDS-PAGE. ABP binds to actin filaments with a K_{app} of 1 μ M and a capacity of 13.5 actin (monomer) subunits in a filament. After cleavage with calpain, both intact ABP and the 190-kD calpain-fragment pellet with F-actin,

while the 100/90-kD subfragments remain soluble. The binding affinity of the 190-kD fragment for actin, relative to intact protein, is diminished about threefold. By Scatchard analysis, each 190-kD proteolytic fragment had a capacity of about eight actin monomers in filaments.

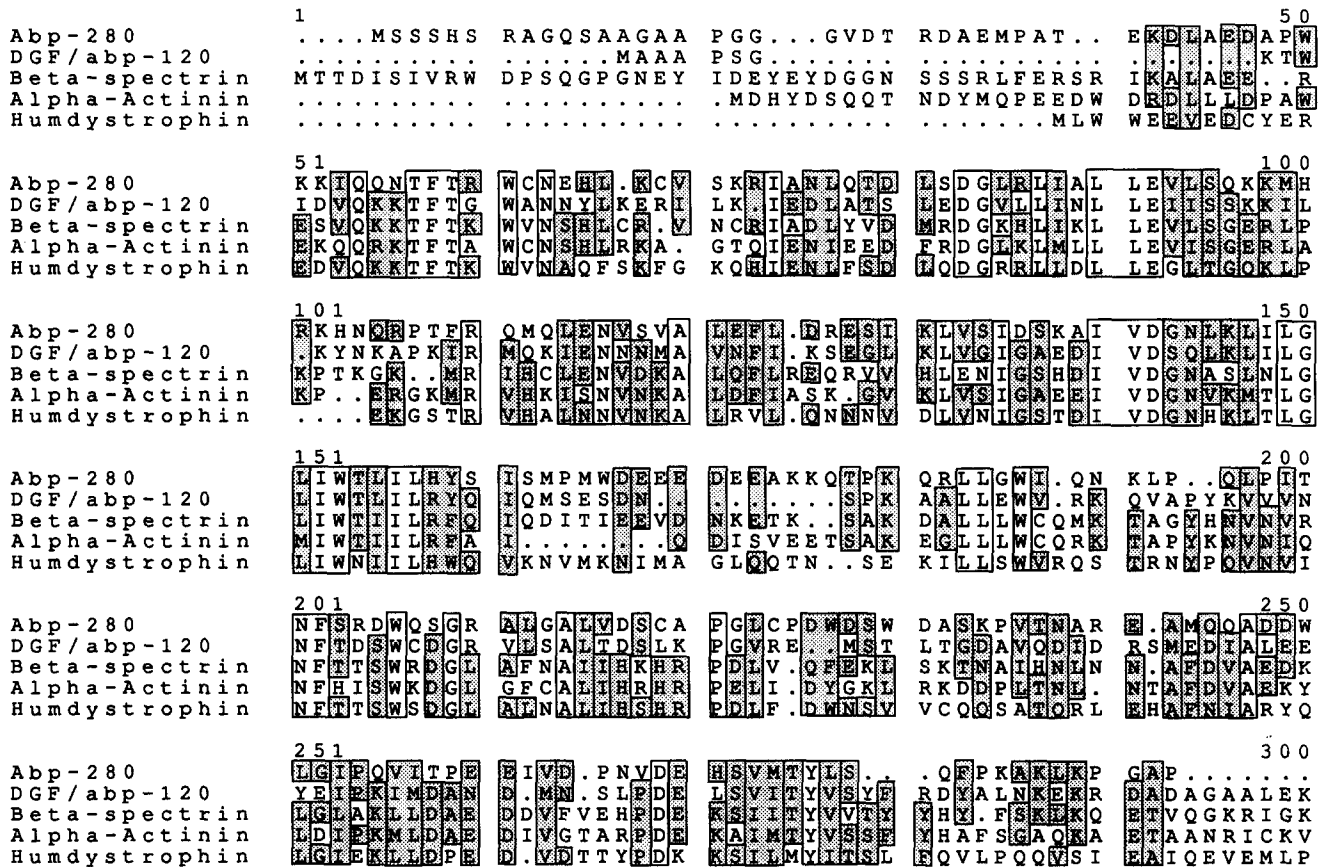


Figure 8. Comparison of ABP's ("ABP-280") amino-terminal 275-amino acid residues to that of *Dictyostelium* abp-120, *Drosophila* β -spectrin, human α -actinin, and human dystrophin. Residues that are identical for all five sequences are enclosed by unshaded boxes. Shaded amino acids are either identical for three or four of the five sequences, or represent conserved substitutions falling into one of the following permutation matrix groups (PIR): D, E, N, Q; F, W, Y, A, G, S, T; H, K, R. Residue numbers correspond to the position of residues within the alignment matrix. Residues beyond 275 of ABP show no significant similarity to β -spectrin, α -actinin or dystrophin. These sequence data are available from EMBL/GenBank/DDBJ under accession number 53416.

Secondary Structure Prediction for the 96-Residue Repeating Motif

The amino acid sequence of the rod domain and its 96-residue repeating motif were analyzed using a series of computer methods that make predictions for secondary structure. Generally similar predictions were obtained with all methods, indicating that the features addressed were probably genuine characteristics of the ABP sequence rather than properties peculiar to the prediction algorithm used. Within each motif was a pattern of seven or eight short spans of residues with a high potential for β - or extended structure, separated by clusters of four or five residues such as glycine, proline, and asparagine that have a high probability of being located within turns. Fourier analysis (Fig. 10) confirmed the presence of the 96-residue repeat and indicated a degree of internal regularity within it. Thus, the Fourier transform of the β -potential along the rod sequence (Fig. 10 a) showed very strong peaks of intensity at frequencies corresponding to the eighth and ninth orders of the fundamental 96-residue repeat. As discussed previously (41), the appearance of such strong intensity at higher orders of the repeat indicates that the internal pattern of β -potential within each 96-residue motif has a regular substructure, with units spaced ~ 12 residues apart. This can be seen in filtered traces of β -potential (Fig.

10 b), which were produced using computer methods analogous to those used to enhance the structural information present in electron micrographs of regular biological objects (see reference 52 for a review). In these filtered traces there were a series of 8 maxima (96/12) each separated by ~ 12 residues.

A similar pattern was detected for turn potential, although the pattern of turn potential within a subunit was out of phase with that for β -structure, so that when turn potential was high, β -potential was low and vice versa. As illustrated in Fig. 9 b, this pattern correlated directly with the sequence, where eight zones, labeled A through H, could be identified. Each zone contained a series of residues of high β -potential (such as phenylalanine, leucine, isoleucine, valine and tyrosine) followed by a series of turn predictors. The pattern was most marked in zones D through H, whereas zone B had the most variable sequence and weakest correlation with the predicted pattern of secondary structure. This variation in the strength of the pattern between zones was also reflected in the filtered traces, where the pattern of β -potential alternating with turns was strongest for zones D-H (see Fig. 10 b). Within the predicted runs of β -structure there was frequently a pattern of alternating hydrophobic and hydrophilic amino acid side chains, similar to that observed with *Dictyostelium* abp-120 (41). This pattern was particularly strongly

conserved between repeats as shown in Fig. 9 *b* by alternating aqua (hydrophilic) and magenta (hydrophobic) residues. In this figure, turn residues are represented in green. The greatest degree of conformity to the consensus repeat was found within repeats 1–15 and repeats 17, 19, 21, and 23. The amino-terminal portions of repeats 16, 18, 20, 22, and 24 (as aligned in Fig. 9 *b*) showed the greatest divergence from the consensus. The predominance of predicted β -secondary structure in the repeating motifs of the ABP rod was consistent with the 50–70% content of β -secondary structure and absence of α -helical structure observed by both circular dichroism and infrared spectroscopy for purified chicken gizzard smooth muscle filamin (31).

Self-Association of ABP Involves a Region within the Most Carboxy-Terminal 96-Residue Repeat Motif

EM (26) has shown that the self-association of ABP monomers occurs at the opposite end to where the monomer binds actin. Because the actin-binding domain is located near the amino terminus, the dimerization domain (or “tail”) must reside near the carboxy terminus. This hypothesis is consistent with previously published data that showed that the 100-kD calpain fragment (which mAb mapping showed derived from the carboxy-terminal region of the sequence) could be chemically crosslinked to form dimers (64). To define the region required for self-association, we expressed two carboxy-terminal constructs as secreted fusion proteins in Cos cells. Both constructs began at residue 2,281 in the middle of repeat 21 (zone *E* in Fig. 9 *b*). The former construct included the natural carboxy terminus (21E–24H). The latter construct had the carboxy-terminal 65 residues deleted (by cleavage at the Pst I site, Fig. 11 *a*), which removed the zones with strongest predicted β -sheet structure (21E–24C). Expression was mediated by the CMD8 plasmid that initiated transcription within the 5' portion of plasma gelsolin cDNA (encoding the extension peptide required for secretion and plasma extension of gelsolin [33]) ligated to ABP cDNA encoding the carboxy-terminal residues of ABP. Chemical cross-linking with DMA (which cross-links native ABP effectively (61, 64) (Fig. 11 *b*) showed that only the construct including the complete carboxy terminus (21E–24H), but not the construct missing the last 65 residues of repeat 24 (21E–24C), cross-linked to a dimer that migrated at twice the size of the original construct. ABP's most carboxy-terminal 65 residues are therefore critical for dimerization. Although it is conceivable that the hexapeptide RSRPRL encoded at the carboxy terminus of the fusion protein might inhibit either self-association or DMA-mediated cross-linking, this would not negate the implication that the structure of the 24th repeat is critical to self-association.

mAbs 1 and 2 did not bind to the expressed construct of residues 2,282–2,647, consistent with their observed binding to the β -galactosidase fusion protein encoded by clone 2 containing residues 1,290–2,029 (Fig. 1). Because these two mAbs bound to the 100-kD calpain fragment that begins at residue 1,762, the epitopes recognized by these mAbs must reside between residues 1,762 and 2,029 (see Fig. 4 *c*).

Discussion

In electron micrographs, rotary shadowed molecules of ABP have a contour length \sim 160 nm and appear as pairs of thread-

like strands, linked at one end, which we have designated the tail (26). The opposite ends, defined as heads, contain actin filament binding sites. The region near the head is flexible and acquires a large variety of configurations, including the appearance of rolling into globular structures. The remainder of the strand appears more uniform in contour and includes straight segments that appear to rotate with respect to one another as if connected by two universal joint-type hinges. The first such hinge is \sim 55 nm from the head; the second is located \sim 15 nm distal to the first, near where the tails join. Strands tend to separate from each other at an acute angle giving the junction and the overall configuration of the dimer a V shape. Rotation at the apparent hinges, and between each backbone repeat segment, may permit ABP to contort, allowing the actin-binding sites to attach to the same actin filament or to link actin filaments at right angles (26). The primary structure of ABP reported in this paper reveals features that permit a first approximation as to why it exhibits this morphology and how it functions as a potent actin-cross-linking and actin-integral membrane protein-ligating agent.

The Actin-binding Domain

The orientation determined for the ABP subunit indicated that the actin-binding head is near its amino terminus, and that this region is similar to putative actin-binding domains of other actin filament-binding proteins. These regions have been identified as putative actin-binding sites by actin-filament cosedimentation studies on proteolytic (29) or selectively expressed fragments in several of these proteins. A recent study, fragmenting the *Dictyostelium* abp-120 with trypsin, showed that a cleavage resulting in the loss of residues 89 through 115 of the *Dictyostelium* protein correlates with the loss of actin-binding activity (5). Fragments generated by trypsin or by calpain encompassing the amino-terminal 90-kD or \sim 840 residues of the ABP subunit bind actin filaments, but genetically engineered polypeptides containing residues 183–689, e.g., beginning \sim 20 kD from the amino-terminus of ABP did not. Therefore, if the expressed hybrid protein achieved native conformation, it can be inferred that actin-binding by ABP requires the first 20 kD of amino-terminal sequence.

The Rod and Tail Domains

General Structure of the Rod and Tail. The rod and tail contain 24 repeating motifs averaging 96 residues each. The motifs in turn consist of 6–8 runs of 6–9 residues with predicted β -sheet structure spaced \sim 12 residues apart interspersed with 3–4 amino acids with high turn potential. Self-association requires a domain in the last half of the last repeat as shown by the ability to cross-link a polypeptide including the last four repeats, but failure to cross-link one missing the last 65 residues.

A Model for the Rod and Tail. Although any conclusions regarding higher order structure based on primary amino acid sequence must be tentative, it is possible to construct an attractive if not exclusive model to explain how the 96-amino acid repeats assemble in the ABP subunits. First, as a general principle, the series of 24 β -sheet repeats, provides a system of building blocks to construct a long strand whose mechanical properties are determined by how the blocks orient with respect to one another within the subunit

and with respect to those in the paired strand of the dimer. The first 15 sequence repeats have the greatest regularity, consistent with their location within the region where the strands are separated from one another, and in a fashion that facilitates intrachain pairing. The sequence similarity and the strength of the predicted β -sheet structure of these repeats is strongest in the first β -sheet run (A) and the third through eighth runs (C-H) (Fig. 9 b). Run B in each motif has the lowest β -sheet potential and may instead be a flexible linker region between functional repeat units offset from the sequence repeat. β -secondary structure is formed by hydrogen bonding between peptide backbones of adjacent chains having this conformation (11). Amino acid side chains project perpendicular to the plane of the backbone, and since residues in each stretch of β -sheet in ABP characteristically alternate hydrophobic and hydrophilic side chains, the resultant β -sheet zones have both hydrophilic and hydrophobic faces. Our model for orienting the hydrophobic and hydrophilic faces therefore incorporates a functional unit offset from the repeat unit, with partial disruption of β -sheet structure near the carboxy-terminal repeats, freeing some of the hydrophobic faces of one subunit to interact with corresponding faces from the other. The hydrophobic faces of regions C-H of one repeat and region A of the next repeat might fold onto themselves, forming a hydrophobic core. A model with this construction yields a series of staggered building blocks shown in Figs. 4 c and 12.

As the sequence approaches the tail, it changes in two ways. First, two intervening amino acid insertions before repeats 16 and 24 interrupt the repeat structure to establish hinges, discussed in greater detail below. Second, the amino-terminal half of even repeats, from number 16 through 24, diverge from the consensus repeat. Repeat 18 is notable for an apparent deletion of nine amino acids and repeats 20 and 22 each contain a cluster of positive charged residues in lieu of runs A and B within the repeat. The effect of each of these modifications may be to disrupt the alternating neighbor interaction characteristic of repeats 1 through 16 and to create unpaired hydrophobic faces. As a result, the hydrophobic faces of the repeats are able to interact with their counterparts in the opposite strand, thereby producing self-association (as detailed in Fig. 12b). Alternatively, the large insertion at the beginning of repeat 24 and abrupt termination of the repeat, before the end of a functional repeat, might prevent a final intrachain hydrophobic interaction and shift it to interchain bonding. The last four repeats are sufficient and the last half of the last motif is essential for dimerization, but we cannot rule out some further contribution of repeats 16–20 to this function. The tight linkage of ABP subunits to one another under physiological ionic conditions and inability to be separated by chaotropic agents but rather only by SDS, is consistent with hydrophobic linkage between the subunits (26). Therefore, the deviation from the consensus in the carboxy third of the ABP subunit may contribute to a shift from intrachain to interchain pairing.

An alternative model, in which all of the hydrophobic faces from each β -sheet run within a 96-amino acid repeat share one orientation, was proposed for *Dictyostelium* abp-120, the only other protein in which a β -turn motif structure similar to that in ABP has been observed (41). This model predicts that each \sim 100-residue repeat forms a planar unit with both a hydrophilic and hydrophobic face. As a general

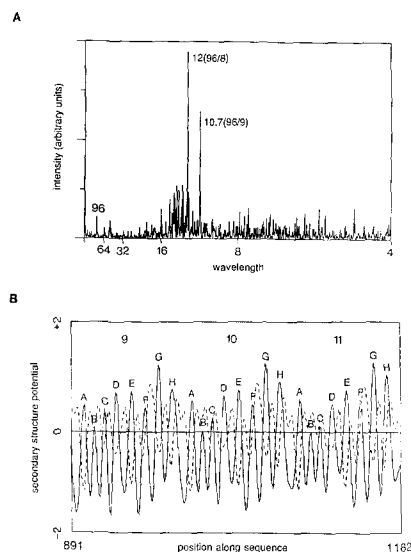


Figure 10. (A) Fourier transform of the β -structure potential along the ABP rod domain. This method expressed the variation of β -potential along the sequence in terms of a sum of cosine wave functions and produced a spectrum of waves. This is analogous to expressing sound waves as a spectrum. Peaks indicated the presence of strong periodicities in the β -secondary structure potential. Analogous to musical notes, there was both a fundamental frequency (at a wavelength of 96 residues) and a series of overtones. The fundamental frequency corresponded to the 96-residue repeating motif detected by the dotplot analysis in Fig. 9 a. The 8th and 9th overtones were particularly strong and corresponded to wavelengths of 12 and 10.7 amino acid residues, respectively. This indicated that within each 96-residue motif, there was an internal fine structure in the β -potential that repeated about eight times. (B) Filtered trace of the variation of β -potential (full lines) and turn potential (broken lines) along the ABP sequence. This filtered trace was produced by using information near the overtone peaks from the respective Fourier transforms with methods analogous to those used to filter electron micrographs of regular biological objects (see reference 52, for review). This filtering averaged the data from all 24 of the 96-residue repeats and showed that the peaks in β -potential were out of phase with those for turns, indicating that the secondary structure of the repeating motif was composed of a series of short runs of β -structure alternating with turns. This figure shows three representative motifs (numbered 9, 10, and 11). Each motif contains eight peaks in β -potential which correlates with the eight zones labeled A through H identified in Fig. 9 b. The peaks vary in size correlating with the strength of predicted β -potential. Zones D-H have the strongest predicted β -potential, whereas zone "B" has the weakest.

rule, such hydrophobic faces must either pair with neighbors, pair across chains, or fold back on themselves, forming U-shaped structures stabilized by a hydrophobic core. Hence the \sim 100-residue repeat might be planar or it might be folded. If planar, each repeat could pair with a contiguous repeat on the same strand or might interact with a repeat on the opposite strand. If folded, the functional unit would resemble a bead on a string. The model proposed for *Dictyostelium* abp-120 has antiparallel dimeric structure with almost complete overlap of the repeating cross- β -sheet motifs that lie in a coplanar orientation, allowing the hydrophobic faces of the repeating units from one strand to interact with corresponding faces from the other monomer. For human ABP, a planar orientation of seven to eight antiparallel runs

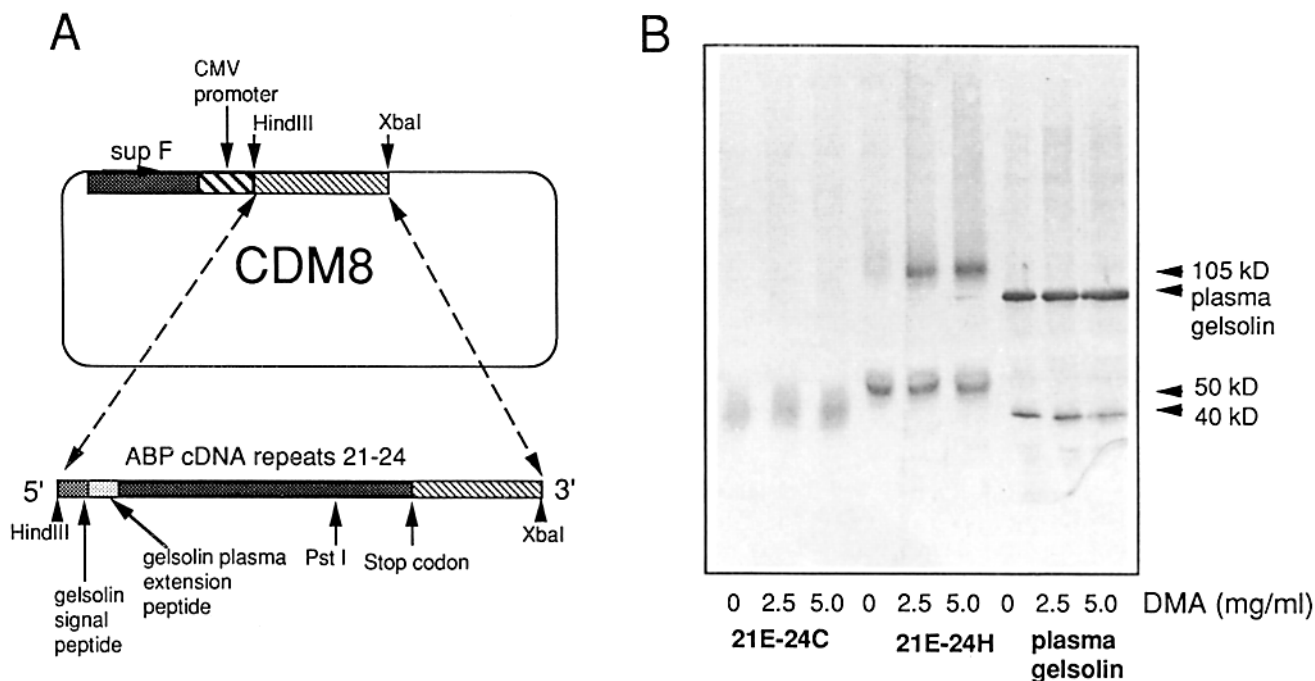


Figure 11. Chemical cross-linking of hybrid proteins including truncates of ABP's carboxy terminus (21E-24H and 21E-24C) expressed by Cos cells demonstrate that self-association requires the last 65 residues. (A) Cos cells were transfected with the CDM8 plasmid vector that included the 5' portion of plasma gelsolin cDNA, (the portion encoding its signal peptide and plasma extension, linked to ABP cDNA encoding ABP's carboxy terminus: motifs 21-24). The fusion protein's amino-terminal signal sequence is cleaved off during secretion leaving 12 residues from plasma gelsolin's amino-terminal extension connected to the amino terminus of the ABP truncate. These residues are recognized by a polyclonal anti-plasma gelsolin antibody. Two carboxy-terminal constructs were made each linking the middle of repeat 21 (ABP residue 2,282) to the plasma gelsolin sequences. The former construct (21E-24H = residues 2,282-2,647) ended at ABP's native stop codon whereas the latter construct (21E-24C, residues 2,282-2,582) deleted ABP's 65 carboxy-terminal residues by cutting at the Pst I site (base ~7,915 in Fig. 3) and ligating to a Pst I site in CDM8. Transcription of the latter construct was terminated by an in-frame stop codon encoded by CDM8 after 18 nucleotides (encoding the hexapeptide RSRPRL). (B) Demonstration that self-association requires an intact last repeat. The first lane in each set of three lanes includes the uncross-linked expressed construct and the second and third lanes in each set of three lanes are after two hours of crosslinking with two concentrations of DMA, a reagent that crosslinks native ABP (61, 64). Lanes 1-3 are the ABP truncate (21E-24C) missing the last half of the last repeat, which on SDS-PAGE ran ~40 kD. Lanes 4-6 show the fusion protein including ABP's native carboxy terminus (21E-24H), migrating at ~50 kD. Lanes 7-9 show plasma gelsolin expressed in an identical fashion in Cos cells, running at 93 kD. Only the fusion protein including ABP's native carboxy terminus (21E-24H) crosslinked, resulting in a polypeptide migrating at 105 kD (lanes 8 and 9), about twice the size of the original construct. Neither the ABP construct deleted at the carboxy terminus, nor the native gelsolin self-associate sufficiently to allow cross-linking.

of eight to nine amino acids with β -sheet structure predicts $3.0\text{--}3.5 \times 2.8\text{--}3.0 \times 1.5$ nm dimensions per planar unit motif. Such an antiparallel dimer model requiring overlap of all 24 repeating units in ABP predicts a molecule of end-to-end distance considerably shorter than ABP's actual contour length of 160 nm (26).

In addition, despite a general similarity in motif structure, a number of differences exist between ABP and *Dictyostelium* abp-120. Fourier analysis suggests that the β -sheet runs within each repeat are shorter and more numerous in the *Dictyostelium* protein and fail to show the sequence degeneracy found between ABP repeat motifs at the carboxy terminus. These differences may be sufficient to alter the mode of motif-motif and monomer-monomer interactions. Further evidence for structural differences between the two proteins is the observation that ABP does not share the aberrancy of migration on electrophoresis in dodecyl sulfate reported for *Dictyostelium* abp-120 (13, 41). The open reading frame of *Dictyostelium* abp-120 cDNA predicts a polypeptide of M_r 92,200, whereas the mature protein migrates with proteins of M_r 120,000 (explaining its name). ABP cDNA predicts a

polypeptide subunit of 280 kD, and physical measurements lead to a similar value (26). Finally, electron micrographs of *Dictyostelium* abp-120 are reportedly consistent with dimerization by antiparallel overlap of the polypeptides along their contour length in contrast to all of the evidence showing that ABP monomers interact only at their carboxy termini (41).

The Hinges. Excluding the entire amino-terminal head, sequence insertions before repeats 16 and 24 deviate most noticeably from the high degree of internal sequence conservation. The finding that calpain, which proteolyzes on the basis of secondary and tertiary protein structure, cleaved the ABP subunits at these sites, suggests the presence of a unique structure at the insertions and is consistent with the hypothesis that they represent discontinuities observed in electron micrographs of ABP strands. Calpain proteolysis studies of platelet GPIb/IX-ABP complexes indicate that GPIb/IX binding takes place within the carboxy-terminal 100 kD of the ABP subunit, and removal of the ultimate 10 kD abrogates this binding. The GPIb/IX binding site must therefore locate near the insertion before motif 24. The presence of the second hinge at that site produced by extension of the poly-

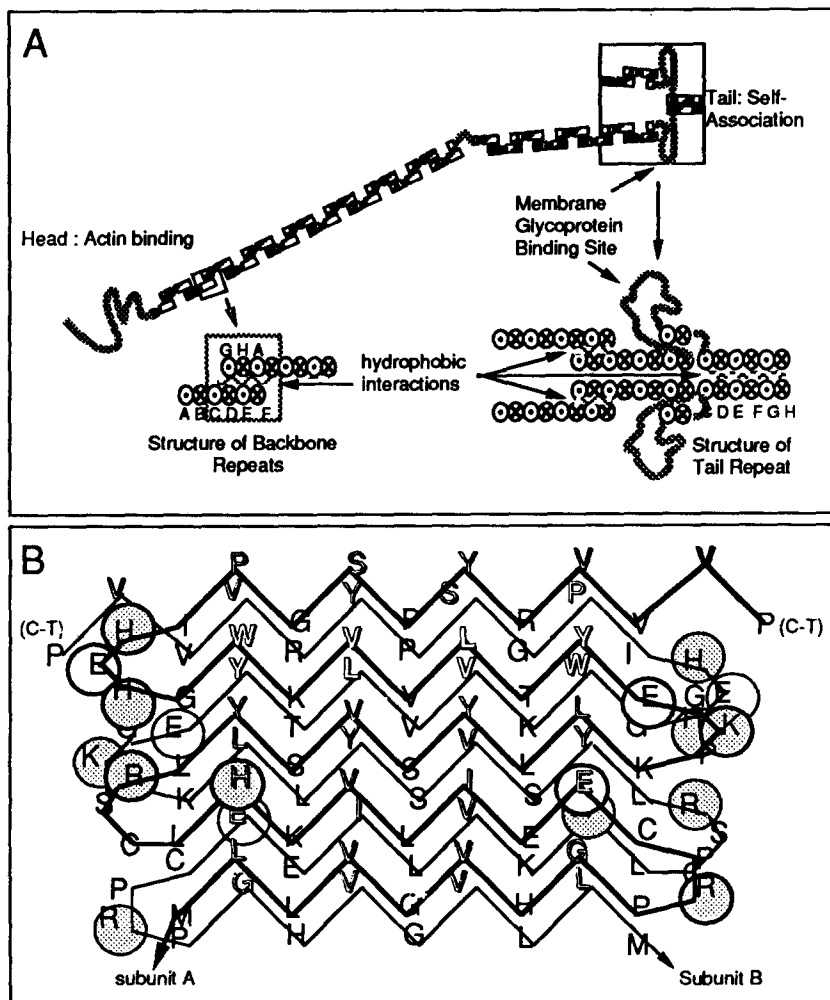


Figure 12. (A) Diagram showing the proposed arrangement of cross- β -sheets within repeats forming the backbone of the ABP molecule and changes that contribute to generation of the self-association site at the last half of repeat 24. The backbone of the molecule is formed out of the 23 repeat units having the functional repeat subunit offset from the sequence repeat shown in Fig. 9 b. Repeats in the backbone may join in the following fashion: a planar hydrophobic face is formed by alignment of the hydrophobic faces of β -sheet zones C to F. Each zone of the cross- β -sheet is indicated by a circle. Circles with dots and X's at their centers represent antiparallel β -sheets running into or out of the plane of the paper, respectively (i.e., cross- β -sheets). The hydrophobic face formed on one side of the planar sheet from zones C-F interacts with a hydrophobic face presented by zones G and H of the same repeat and run A of the next repeat. This pattern of intrachain repeat bonding establishes the backbone from motifs 1-23, although it is interrupted by the insertion before motif 16. The large insertion before the terminal repeat disrupts the overlapping bonding pattern and creates an unpaired hydrophobic face formed by the β -sheet zones C-H in motif 24. This creates a self-association site by allowing pairing between corresponding hydrophobic faces of each 24th repeat. (B) Parallel alignment of the two hydrophobic faces formed by β -sheet runs D to H in motif 24. In this diagram, the shadowed residues indicate alternating residues on the hydrophobic faces of the motif. Charged residues that interrupt the hydrophobic face are indicated by circles (clear circles, negatively charged, darkened circles, positively charged). Most charged residues locate near turns. A parallel orientation of ABP monomers is shown as ionic interactions between the few charged residues neutralize apparent disruptions of the hydrophobic face.

peptide chain away from the backbone of repeat β -sheets could present a binding site to membrane glycoproteins.

Phosphorylation Sites. In view of the observed phosphorylation of ABP *in vivo* and *in vitro* (8, 9, 59, 67), the primary structure was examined for phosphorylation site consensus sequences. A cAMP-dependent kinase phosphorylation was identified at residues 2,147-2,152 in motif 20 and a Ca^{2+} /calmodulin kinase phosphorylation site at residues 2,520-2,523 in the amino acid insertion before motif 24. These findings are provocative, since phosphorylation at the first site might affect the ability of calpain to hydrolyze the ABP subunit at the first hinge, and could explain how cAMP kinase-mediated phosphorylation of ABP reportedly increases its resistance to calpain proteolysis (9). Phosphorylation might neutralize the clusters of positive charges at the beginnings of repeats 20, allowing the subunits to come together. The locations of the second site suggests it may regulate the interaction of ABP with membrane glycoproteins.

ABP as a Leaf Spring: the ABP Subunit Structure and Actin Cross-linking

The large extension and high radius of gyration documented

for ABP were proposed as prerequisites for the efficient cross-linking of actin filaments by ABP, because they permit the actin-binding domains in the heads of the strands to locate and then fit firmly along the helix groove of adjacent actin filaments (37) or even the same filament (26). It is noteworthy that other proteins with similar amino-terminal sequences that bundle actin filaments, namely the subunits of α -actinin, β -spectrin and *Dictyostelium* abp-120, all form antiparallel dimers. These dimers appear as straight rods in the electron microscope, suggesting that although the individual strands might be flexible, they acquire rigidity by overlapping antiparallel pairing with their partners. Furthermore, dimer overlap in the cases of α -actinin and spectrin allow for actin filament binding to be regulated by calcium since the actin-binding region on one strand is covered by an EF hand region belonging to the opposing strand. ABP deviates from this pattern in that its actin-binding sites reside at the ends of free strands, consistent with the observation that neither Ca^{2+} , nor phosphorylation state regulate filament binding. Most of ABP's backbone appears less flexible than its head, but because of its extended length, free rotation between the building blocks could contribute significantly to overall flexibility. Finally, the hinges observed in electron micrographs

and localized in the primary sequence, provide points where the molecule could swivel considerably.

Flexibility, though necessary, is not sufficient to explain how ABP promotes nearly perpendicular interactions of cross-linked actin filaments, because this function requires constraints of movement to maintain high-angle branching. The proposed model exhibits progression from intrachain to interchain hydrophobic interactions between building blocks constructed from β -sheet repeats. This creates a bivalent leaf spring whose leaves are joined firmly at one end. In addition to the interchain interactions that produce self-association at the ultimate carboxy terminus of ABP, additional bonding within repeat domains 16–23 could act to stabilize the separation angle of the subunits by zipping the subunits together in this region. Interspecies differences between the sequences encoding the hinges, the carboxy-terminal repeats, or regions subjected to posttranslational modifications such as phosphorylation, could explain the consistently greater actin gelation potency observed for ABP from rabbit macrophages (6), amphibian oocytes (15), and human uterus (Egan, S., and J. H. Hartwig, unpublished observations) as compared with ABP/filamin from chicken gizzard (6, 14, 42, 45).

The large amino-terminal fragment generated by calpain bound to F-actin with reduced avidity compared with that of native ABP (Fig. 7), but the diminution in binding affinity was much less than would be predicted from conversion of a bivalent ligand to a monovalent one (46). This result is also consistent with the proposed leaf spring model. Tension generated by the zipping together of subunits at the self-association region might functionally reduce the binding avidity of the bivalent species for actin filament in comparison with a monovalent subunit not so constrained. An increased capacity of monomers for actin also suggests that additional, low-affinity actin-binding sites exist on ABP. As dimers, ends of molecules are bound to different actin filaments. Filament motions would extend ABP strands, diminishing the amount of each strand making contact with actin. In a relaxed state (monomer), more of the ABP strand could contact the actin filament, stabilizing the ABP-filament bond. ABP may therefore bind actin initially using its widely separated amino-terminal binding sites. Binding of additional actin monomers along the filament could help stabilize the branched configuration.

The authors are grateful to B. Seed for gifts of Cos cells and the CDM8 vector. We also thank Michelle DeSisto and Mark Kozam for the excellent technical help and Darlene M. Jackson for editorial assistance.

Received for publication 3 April 1990 and in revised form 1 June 1990.

References

1. Baron, M., M. Davison, P. Jones, and D. Critchley. 1987. The sequence of chick α -actinin reveals homologies to spectrin and calmodulin. *J. Biol. Chem.* 262:17623–17629.
2. Blackshear, P., A. Nairn, and J. Kuo. 1988. Protein kinases 1988; a current perspective. *FASEB (Fed. Am. Soc. Exp. Biol.) J.* 2:2958–2969.
3. Boxer, L., and T. Stossel. 1976. Isolation and properties of actin, myosin, and a new actin-binding protein of chronic myelogenous leukemia leukocytes. *J. Clin. Invest.* 57:5696–5705.
4. Boxer, L., S. Richardson, and A. Floyd. 1976. Identification of actin-binding protein in membrane of polymorphonuclear leukocytes. *Nature (Lond.)* 263:249–251.
5. Bresnick, A., V. Warren, and J. Condeelis. 1990. Identification of a short sequence essential for actin binding by *Dictyostelium* ABP-120. *J. Biol. Chem.* In press.
6. Brotschi, E., J. Hartwig, and T. Stossel. 1978. The gelation of actin by actin-binding protein. *J. Biol. Chem.* 253:8988–8993.
7. Byers, T., A. Husain-Chishti, R. Dubreuil, D. Branton, and L. Goldstein. 1989. Sequence similarity of the amino-terminal domain of *Drosophila* beta spectrin to alpha actinin and dystrophin. *J. Cell Biol.* 109:1633–1641.
8. Carroll, R., and J. Gerrard. 1982. Phosphorylation of platelet actin-binding protein during platelet activation. *Blood.* 59:466–471.
9. Chen, M., and A. Stracher. 1989. *In situ* phosphorylation of platelet actin-binding protein by cAMP-dependent protein kinase stabilizes it against proteolysis by calpain. *J. Biol. Chem.* 264:14282–14289.
10. Chirgwin, J., A. Przybala, R. MacDonald, and W. Rutter. 1979. Isolation of biologically active ribonucleic acid from sources enriched in ribonuclease. *Biochemistry.* 18:5294–5299.
11. Chothia, C. 1983. Coiling of beta-pleated sheets. *J. Mol. Biol.* 163:107–117.
12. Chou, P., and G. Fasman. 1978. Prediction of the secondary structure of proteins from their amino acid sequence. *Adv. Enzymol. Relat. Areas Mol. Biol.* 47:45–148.
13. Condeelis, J., M. Vahey, J. M. Carboni, J. DeMey, and S. Ogihara. 1984. Properties of the 120,000- and 95,000-dalton actin-binding proteins from *Dictyostelium discoideum* and their possible functions in assembling the cytoplasmic matrix. *J. Cell Biol.* 99:119s–126s.
14. Cortese, J. D., and C. Frieden. 1988. Microheterogeneity of actin gels formed under controlled linear shear. *J. Cell Biol.* 107:1478–1487.
15. Corwin, H. L., and J. H. Hartwig. 1983. Isolation of actin-binding protein and villin from toad oocytes. *Dev. Biol.* 99:61–74.
16. Dorfman, D., L. Zon, and S. Orkin. 1989. Rapid amplification of λ gt11 bacteriophage library inserts from plaques using the polymerase chain reaction (PCR). *Bio Techn.* 569–570.
17. Deleted in proof.
18. Ezzell, R., D. Kenney, S. Egan, T. Stossel, and J. Hartwig. 1988. Localization of the domain of actin-binding protein that binds to membrane glycoprotein Ib and actin in human platelets. *J. Biol. Chem.* 263:13303–13309.
19. Deleted in proof.
20. Fox, J. 1985. Identification of actin-binding protein as the protein linking the membrane skeleton to glycoproteins on platelet plasma membrane. *J. Biol. Chem.* 260:11970–11977.
21. Fox, J., C. Reynolds, and D. Phillips. 1983. Calcium-dependent proteolysis occurs during platelet aggregation. *J. Biol. Chem.* 258:9973–9981.
22. Ginsberg, D., R. Handin, D. Bonthron, T. Donlon, G. Bruns, S. Latt, and S. Orkin. 1985. Human von Willebrand factor (VWF): isolation of complementary DNA (cDNA) clones and chromosomal localization. *Science (Wash. DC)* 228:1401–1406.
23. Hammonds, R. 1987. Protein sequence of DMD gene is related to actin-binding domain of α -actinin. *Cell.* 51:1.
24. Hartwig, J., and P. Shevlin. 1986. The architecture of actin filaments and the ultrastructural location of actin-binding protein in the periphery of lung macrophages. *J. Cell Biol.* 103:1007–1020.
25. Hartwig, J., and T. Stossel. 1975. Isolation and properties of actin, myosin, and a new actin-binding protein in rabbit alveolar macrophages. *J. Biol. Chem.* 250:5696–5705.
26. Hartwig, J., and T. Stossel. 1981. The structure of actin-binding protein molecules in solution and interacting with actin filaments. *J. Mol. Biol.* 145:563–581.
27. Hartwig, J., J. Tyler, and T. Stossel. 1980. Actin-binding protein promotes the bipolar and perpendicular branching of actin filaments. *J. Cell Biol.* 87:841–848.
28. Henikoff, S. 1984. Unidirectional digestion with exonuclease III creates targeted breakpoints for DNA sequencing. *Gene (Amst.)* 28:351–359.
29. Imamura, M., T. Endo, M. Kuroda, T. Tanaka, and T. Masaki. 1988. Substructure and higher structure of chicken smooth muscle α -actinin molecule. *J. Biol. Chem.* 263:7800–7805.
30. Janmey, P. A., S. Hvidt, J. Lamb, and T. P. Stossel. 1990. Resemblance of actin-binding protein/actin gels to covalently crosslinked networks. *Nature (Lond.)* 345:89–92.
31. Kotliansky, V., M. Glukhova, V. Shirinsky, V. Smirnov, T. Bushueva, V. Filimonov, and S. Venyaminow. 1982. A structural study of filamin, a high-molecular-weight actin-binding protein from chicken gizzard. *Eur. J. Biochem.* 121:553–559.
32. Kozak, M. 1984. Compilation and analysis of sequences upstream from the translational start site in eukaryotic mRNAs. *Nucleic Acids Res.* 12:857–872.
33. Kwiatkowski, D., P. Janmey, and H. Yin. 1989. Identification of critical functional domains in gelsolin. *J. Cell Biol.* 108:1717–1726.
34. Lucas, R., M. Gallagher, and A. Stracher. 1976. Actin and actin binding protein in platelets. In *Contractile Systems in Non-muscle Tissues*. S. Perry, editor. Elsevier/North Holland Biomed Press, Amsterdam. 133–139.
35. Maizel, J., and R. Lenk. 1981. Enhanced graphic matrix analysis of nucleic acid and protein synthesis. *Proc. Natl. Acad. Sci. USA.* 78:7665–7667.
36. Maniatis, T., E. Fritsch, and J. Sambrook. 1982. *Molecular Cloning: A Laboratory Manual*. Cold Spring Harbor Laboratory, Cold Spring Harbor, NY.
37. Maruyama, K., and K. Ohashi. 1978. Tropomyosin inhibits the interaction of f-actin and filamin. *J. Biochem. (Tokyo)* 84:1017–1019.

38. Deleted in proof.
39. Messing, J., B. Gronenborn, B. Muller-Hill, and P. Hofschneider. 1977. Filamentous coliphage M13 as a cloning vehicle: insertion of a Hind II fragment of the lac regulatory region in M13 replicative form in vitro. *Proc. Natl. Acad. Sci. USA.* 74:3642-3646.
40. Niederman, R., P. Amrein, and J. Hartwig. 1983. The three dimensional structure of actin filaments in solution and an actin gel made with actin-binding protein. *J. Cell Biol.* 96:1400-1413.
41. Noegel, A., S. Rapp, F. Lottspeich, M. Schleicher, and M. Stewart. 1989. The *Dictyostelium* gelation factor shares a putative actin-binding site with α -actinin and dystrophin and also has a rod domain containing six 100-residue motifs that appear to have a cross- β conformation. *J. Cell Biol.* 108:607-618.
42. Nunnally, M. H., L. D. Powell, and S. W. Craig. 1981. Reconstitution and regulation of actin gelsol transformation with purified filamin and villin. *J. Biol. Chem.* 256:2083-2086.
43. Okita, L., D. Pidard, P. Newman, R. Montgomery, and T. Kunicki. 1985. On the association of glycoprotein Ib and actin-binding protein in human platelets. *J. Cell Biol.* 100:317-321.
44. Robson, B., and E. Suzuki. 1976. Conformations of amino acid residues in globular proteins. *J. Mol. Biol.* 107:327-356.
45. Rockwell, M. A., M. Fechheimer, and D. L. Taylor. 1984. A comparison of methods used to characterize gelation of actin in vitro. *Cell Motil.* 4:197-213.
46. Roitt, I., J. Brostoff, and D. Male. 1989. Immunology. C.V. Mosby Co., St. Louis, MO.
47. Rosenberg, S., A. Stracher, and R. Lucas. 1981. Isolation and characterization of actin and actin-binding protein from human platelets. *J. Cell Biol.* 91:201-211.
48. Sanger, F., S. Nicklen, and A. Coulson. 1977. DNA sequencing with chain-terminating inhibitors. *Proc. Natl. Acad. Sci. USA.* 74:5463-5467.
49. Schollmeyer, J., G. Rao, and J. White. 1978. An actin-binding protein in human platelets. *Am. J. Pathol.* 93:433-445.
50. Seed, B. 1987. An LFA-3 cDNA encodes a phospholipid-linked membrane protein homologous to its receptor CD2. *Nature (Lond.)* 329:840-842.
51. Shizuta, Y., H. Shizuta, M. Gallo, P. Davies, and I. Pastan. 1976. Purification and properties of filamin, an actin-binding protein from chicken gizzard. *J. Biol. Chem.* 251:6562-6567.
52. Stewart, M. 1988. An introduction to the computer image processing of electron micrographs of 2-dimensionally ordered biological structures. *J. Electr. Microsc. Techn.* 9:301-324.
53. Stewart, M., R. Quinlan, R. Moir, S. Clarke, and S. Atkinson. 1989. The role of repeating sequence motifs in interactions between α -helical coiled-coils such as myosin, tropomyosin and intermediate filament proteins. In Springer Advances in Biophysics. P. Bayley, editor. Springer-Verlag, Heidelberg, FRG.
54. Stossel, T. 1989. From signal to pseudopod. How cells control cytoplasmic actin assembly. *J. Biol. Chem.* 264:18261-18264.
55. Stossel, T. P., and J. H. Hartwig. 1976. Interaction of actin, myosin, and a new actin-binding protein of rabbit pulmonary macrophages. II. Role in cytoplasmic movement and phagocytosis. *J. Cell Biol.* 68:602-619.
56. Stossel, T., C. Chaponnier, R. Ezzell, J. Hartwig, P. Janmey, D. Kwiatkowski, S. Lind, D. Smith, F. Southwick, H. Yin, and K. Zaner. 1985. Nonmuscle actin-binding proteins. *Annu. Rev. Cell Biol.* 353-402.
57. Towbin, J., T. Staehelin, and J. Gordon. 1979. Electrophoretic transfer of proteins from polyacrylamide gels to nitrocellulose sheets: procedure and some applications. *Proc. Natl. Acad. Sci. USA.* 76:4350-4354.
58. Tyler, J. M., J. M. Anderson, and D. Branton. 1980. Structural comparison of several actin-binding molecules. *J. Cell Biol.* 85:489-495.
59. Wallach, D., P. Davies, and I. Pastan. 1978. Cyclic AMP-dependent phosphorylation of filamin in mammalian smooth muscle. *J. Biol. Chem.* 253:4739-4745.
60. Wang, K. 1977. Filamin, a new high-molecular-weight protein found in smooth muscle and nonmuscle cells. Purification and properties of chicken gizzard filamin. *Biochemistry.* 16:1857-1865.
61. Wang, K., and S. Singer. 1977. Interaction of filamin with f-actin in solution. *Proc. Natl. Acad. Sci. USA.* 74:2021-2025.
62. Wang, K., J. Ash, and S. Singer. 1975. Filamin, a new high-molecular-weight protein found in smooth muscle and non-muscle cells. *Proc. Natl. Acad. Sci. USA.* 72:4483-4486.
63. Weihing, R. 1983. Purification of HeLa cell high molecular weight actin binding protein and its identification in HeLa cell plasma membrane ghosts and intact HeLa cells. *Biochemistry.* 22:1839-1847.
64. Weihing, R. 1988. Actin-binding and dimerization domains of HeLa cell filamin. *Biochemistry.* 27:1865-1869.
65. Deleted in proof.
66. Youssoufian, H., M. McAfee, and D. Kwiatkowski. 1990. Cloning and chromosomal localization of the human cytoskeletal α -actinin gene reveals linkage to the β -spectrin gene. *Am. J. Hum. Genet.* 47:62-72.
67. Zhang, A., J. Lawrence, and A. Stracher. 1988. Phosphorylation of platelet actin binding protein protects against proteolysis by calcium dependent protease. *Biochem. Biophys. Res. Commun.* 151:355-360.